Redox Biology 36 (2020) 101631

Contents lists available at ScienceDirect

Redox Biology

journal homepage: www.elsevier.com/locate/redox

Research Paper

Peroxynitrous acid (ONOOH) modifies the structure of anastellin and influences its capacity to polymerize fibronectin

Jianfei He [a], Eva Ramos Becares [a], Peter Waaben Thulstrup [b], Luke F. Gamon [a], Jannik Nedergaard Pedersen [c], Daniel Otzen [c], Pontus Gourdon [a], Michael J. Davies [a,*,1], Per Hägglund [a,1,*]

[a] Department of Biomedical Sciences, University of Copenhagen, Copenhagen, Denmark
[b] Department of Chemistry, University of Copenhagen, Copenhagen, Denmark
[c] Interdisciplinary Nanoscience Center (iNANO), Department of Molecular Biology and Genetics, Aarhus University, Aarhus, Denmark

ARTICLE INFO

Keywords:
Anastellin
Extracellular matrix
Fibronectin
Peroxynitrous acid
Protein oxidation
Aggregation

ABSTRACT

Anastellin (AN), a fragment of the first type III module in fibronectin (FN), initiates formation of superfibronectin, a polymer which resembles the native cell-derived fibrillar FN found in the extracellular matrix of many tissues, but which displays remarkably different functional properties. Here we demonstrate that exposure of AN to the biologically-important inflammatory oxidant, peroxynitrous acid (ONOOH), either as a bolus or formed at low levels in a time-dependent manner from SIN-1, impairs the capability of AN to polymerize FN. In contrast, exposure of FN to ONOOH does not seem to affect superfibronectin formation to the same extent. This oxidant-induced loss-of-function in AN occurs in a dose-dependent manner, and correlates with structural perturbations, loss of the amino acid tyrosine and tryptophan, and dose-dependent formation of modified amino acid side-chains (3-nitrotyrosine, di-tyrosine and 6-nitrotryptophan). Reagent ONOOH also induces formation of oligomeric species which decrease in the presence of bicarbonate, whereas SIN-1 mainly generates dimers. Modifications were detected at sub-stoichiometric (0.1-fold), or greater, molar excesses of oxidant compared to AN. These species have been localized to specific sites by peptide mass mapping. With high levels of oxidant (>100 times molar excess), ONOOH also induces unfolding of the beta-sheet structure of AN, thermal destabilization, and formation of high molecular mass aggregates. These results have important implications for the understanding of FN fibrillogenesis *in vivo*, and indicates that AN is highly sensitive to pathophysiological levels of oxidants such as ONOOH.

1. Introduction

Fibronectin (FN) is a dimeric multimodular glycoprotein present *in vivo* as two different isoforms: a soluble form in blood plasma, and as an insoluble form generated by endothelial, epithelial and fibroblast cells, that contains additional modules. The latter forms fibrils in the extracellular matrix (ECM) – the scaffold that provides strength and form to most biological tissues. Each monomer is composed of domains of repeating type I (FNI), II (FNII), and III (FNIII) modules which provide different functionalities and binding sites for a variety of biomacromolecules, including integrins, collagen, heparin, and proteoglycans [1,2]. The circulating soluble form produced by hepatocytes is recruited to sites of injury where it is cross-linked with fibrinogen to form a temporary scaffold for attachment of cells involved in repair and wound healing [3]. The fibrillar form of FN derived from cells involved in matrix synthesis such as fibroblasts, endothelial cells and smooth muscle cells, plays an important role in cell adhesion and migration, and has a strong influence on tumor growth, angiogenesis and metastasis [4,5]. The process of FN fibrillogenesis in the ECM is not fully understood but strong evidence supports involvement of interactions between FN and integrin receptors on the cell surface [6]. Cell contraction mediated by the cytoskeleton exerts a pulling force on FN

Abbreviations: AN, anastellin; di-Tyr, dityrosine; ECM, extracellular matrix; FN, fibronectin; sFN, superfibronectin; 6-nitroTrp, 6-nitrotryptophan; 3-nitroTyr, 3-nitrotyrosine; ThT, thioflavine T.

* Corresponding authors.
E-mail addresses: davies@sund.ku.dk (M.J. Davies), pmh@sund.ku.dk (P. Hägglund).
[1] Joint senior.

https://doi.org/10.1016/j.redox.2020.101631
Received 16 April 2020; Received in revised form 18 June 2020; Accepted 28 June 2020
Available online 3 July 2020

via integrin receptors which exposes cryptic sites that initiate fibrillation through interactions with proximal FN protomers [7]. Anastellin (AN), a small ~ 9 kDa fragment from the C-terminal part of the first type III module ($FNIII_1$) in FN can initiate formation of so-called superfibronectin *in vitro*, a fibrillar form which resembles ECM FN at the microscopic level, but displays higher cell adhesiveness than regular ECM fibrils and suppresses cell migration [8]. AN lacks the two first β-strands present in $FNIII_1$ and is believed to represent a partially unfolded intermediate with exposed hydrophobic patches that bind to interaction sites in transiently unfolded FN, thereby promoting polymerization [9–11]. AN can also bind to previously assembled FN in the ECM *in vivo*, and thereby modulate the structure of FN and the surrounding ECM [12–14]. These events have been linked to perturbations in cell signaling pathways such as those involving p38, ERK, VEGF, and lysophospholipids [12,15–17]. In addition, AN and superfibronectin display anti-metastatic properties in mice injected with multiple human tumor cell types [18,19]. These functions however appear to be independent of the fibrillation activity of AN since they are not perturbed in a mutant that lacks the ability to form superfibronectin [16,20].

Oxidants such as peroxynitrous acid (ONOOH) and hypochlorous acid (HOCl) are released into the ECM by activated leukocytes and macrophages during inflammation [21]. These oxidants are key components of the innate immune response to invading pathogens, but excessive or unintended formation can also result in damage to host tissues and modify ECM components, including FN [22]. This has functional implications, as cells adhere to ONOOH-modified FN to a much lower extent than native FN, with this occurring in a dose-dependent manner with increasing ONOOH exposure [23]. ONOOH is formed at a diffusion-controlled rate from superoxide ($O_2^{\cdot-}$) generated by NADPH oxidases (and also other processes), and nitric oxide ($NO^{\cdot}$) produced by nitric oxide synthases [24]. ONOOH can either induce oxidation directly, or undergo secondary reactions to form other reactive species. Thus, ONOOH can decompose (to a limited extent) to the reactive radicals $HO^{\cdot}$ and $NO_2^{\cdot}$, or react with CO_2 to form peroxynitrosocarbonate ($ONOOCO_2^-$). The latter can, in turn decompose to $NO_2^{\cdot}$ and $CO_3^{\cdot-}$ [25]. Each of these species can induce damage to a greater or lesser extent. Tyrosine (Tyr) and tryptophan (Trp) residues are major targets of the radicals formed from ONOOH and $ONOOCO_2^-$, resulting in the formation of 3-nitroTyr, 6-nitroTrp, and the cross-linked species di-tyrosine (di-Tyr) [26]. As AN contains several exposed aromatic residues, and few alternative ONOOH-reactive species (e.g. no cysteine or methionine residues), we hypothesized that Tyr and Trp might be major targets in AN for ONOOH and $ONOOCO_2^-$, and that this might modify AN structure and function, with downstream effects on FN polymerization.

2. Materials and methods

2.1. Materials

All chemicals including lyophilized human plasma FN (#F1056) and anti-3-nitroTyr polyclonal antibody (pAb; #06-284) were from Sigma-Aldrich (St Louis, Missouri, USA) unless stated otherwise, and all solutions were prepared with Milli-Q grade water (Millipore Advantage A10; Merck-Millipore, Billerica, MA, USA). Peroxynitrous acid (ONOOH) was synthesized in a two-phase system using isoamyl nitrite/hydrogen peroxide (H_2O_2), with unreacted H_2O_2 removed using manganese dioxide [27]. Stock solutions of ONOOH were stored at -80 °C. Before use, the concentration of ONOOH (diluted in 0.1 M NaOH) was determined by UV–vis spectrophotometry (UV-2600, Shimadzu, Japan) at 302 nm (extinction coefficient 1670 M^{-1} cm^{-1}) [28]. Isopentyl nitrite, 5-amino-3-(4-morpholinyl)-1,2,3-oxadiazolium chloride (SIN-1 chloride), HEPES, NaCl, EDTA, glycerol, β-mercaptoethanol were purchased from VWR. Isopropyl-β-D-thiogalactoside was obtained from Biosynth AG (Staad, Switzerland). Decomposed oxidant solutions (indicated as dONOOH and dSIN-1) were prepared by incubating ONOOH/SIN-1 in 100 mM sodium phosphate buffer (pH 7.4) at 37 °C for 90 min. The anti-6-nitroTrp (clone 117C) and anti-di-Tyr (clone 1C3) monoclonal antibodies (mAb) were from the Japan Institute for the Control of Aging (Shizuoka, Japan). Horseradish peroxidase (HRP)-conjugated sheep anti-mouse secondary antibody and HRP-conjugated donkey anti-rabbit secondary antibody were purchased from VWR. Western lighting Plus-ECL Enhanced chemiluminescence substrate was from Perkin Elmer (USA).

2.2. Production of recombinant anastellin

Escherichia coli codon optimized human AN construct (DNA and encoded protein sequence are available in Supplementary data) was purchased from GenScript Biotech (Leiden, Netherlands). AN was cloned into the vector pET21a+, containing a C-terminal hexahistidine tag (HisTag) for downstream affinity chromatography purification. The construct was transformed into the *E. coli* C43 (DE3) expression strain and cells were grown in Luria-Bertani media at 37 °C until the OD_{600} reached 0.6–0.8. Protein synthesis was induced with 1 mM isopropyl-β-D-thiogalactoside at 15 °C for about 16 h. Cells were harvested by centrifugation at 8000*g* for 15 min, and resuspended at 5 mL g^{-1} wet cells in buffer containing 25 mM HEPES-NaOH, pH 7, 100 mM NaCl, 0.25 mM EDTA, 20% v/v glycerol, 5 mM β−mercaptoethanol, one SIGMAFAST™ protease inhibitor tablet per 6 L culture, and then stored at -20 °C. The thawed cells were passed through a cell disruptor (Constant Systems Limited, Daventry, UK) twice at 25 kpsi, then cell debris were spun down at 20,000 *g* for 40 min, and 2 μg mL^{-1} DNase I and 1 mM phenylmethanesulphonyl fluoride were added. The supernatant from 6 L culture was adjusted to 50 mM imidazole prior to loading on a 5 mL HisTrap HP column (GE Healthcare Life Sciences, Uppsala, Sweden) equilibrated in buffer containing 25 mM HEPES-NaOH pH 7, 100 mM NaCl, 0.25 mM EDTA, 20% v/v glycerol, 5 mM β−mercaptoethanol, using an Äkta pure chromatographic system (GE Healthcare Life Sciences), and eluted with the same buffer containing 500 mM imidazole. Some of the fractions following affinity chromatography purification contained a small amount of precipitate, which was removed by centrifugation at 4500 *g* for 5 min. Protein-containing fractions were pooled, concentrated to 5 mg mL^{-1} on Vivaspin concentrators (molecular mass cut-off: 10 kDa; Sartorius, Göttingen, Germany) and loaded (in 1 mL aliquots), in sequential runs, onto a 24 mL size-exclusion chromatography (SEC) Superdex 75 Increase 10/300 GL column (GE Healthcare Life Sciences) equilibrated with phosphate-buffered saline (PBS, 137 mM NaCl, 2.7 mM KCl, 10 mM Na_2HPO_4 and 1.8 mM KH_2PO_4). The major A_{280} nm peak was collected, assessed for purity by SDS-PAGE, concentrated to 1 mg mL^{-1}, and stored at -80 °C.

2.3. Preparation of modified anastellin and fibronectin

AN (5 μM) was exposed to ONOOH (0–500 μM) or SIN-1 (0–100 μM) in 100 mM phosphate buffer (pH 7.4) for 30 min at 37 °C, in the absence or presence of 25 mM sodium bicarbonate ($NaHCO_3$), prior to analysis by SDS-PAGE, ELISA or mass spectrometry, as described below. For studies of superfibronectin (sFN) formation, AN (40 μM) and FN (0.4 mg mL^{-1}; 1.4 μM) was incubated separately with different concentrations of ONOOH (0–8 mM) for 30 min at 21 °C in 100 mM sodium phosphate buffer (pH 7.4). These conditions were also used for CD spectroscopy and analysis of AN aggregates outlined in sections 2.9−2.11 below. The samples were then buffer exchanged into 10 mM sodium phosphate buffer (pH 7.4) using spin filters (Amicon Ultra-0.5 Centrifugal Filter Unit, 3 kDa), with the protein concentration subsequently determined using the BCA assay. The protein samples were then diluted to the required concentration using 10 mM phosphate buffer (pH 7.4) and centrifuged at 20,000 *g* for 10 min at 4 °C to remove any preformed aggregates.

2.4. Turbidity assay

Turbidity measurements were performed with a Spectra Max® i3x microplate reader to study the effect of oxidation on the kinetics of sFN formation. Native or oxidized AN (40 μM) and FN (0.4 mg mL^{-1}; 1.4 μM), prepared as described in section 2.3, were mixed in a final volume of 100 μL in 10 mM sodium phosphate buffer, pH 7.4. The turbidity of the solution at 550 nm was then measured at 1 min intervals for a period of 40 min at 21 °C.

2.5. Sedimentation assay

Native or oxidized AN (40 μM) and FN (1 μM), prepared as described in section 2.3, were mixed in a final volume of 20 μL in 10 mM sodium phosphate buffer (pH 7.4) containing 5 mM EDTA and incubated overnight at 21 °C. After incubation, the samples were centrifuged at 20,000 *g* for 10 min at 4 °C. The insoluble fibril pellets were then washed with 20 μL 10 mM sodium phosphate buffer (pH 7.4). Some pellets of native AN and FN were subsequently incubated with different concentration of ONOOH (0–800 μM) in 20 μL for 30 min at 21 °C in 100 mM sodium phosphate buffer (pH 7.4). All samples were analyzed by SDS-PAGE under reducing conditions as described below.

2.6. SDS-PAGE, western blotting and ELISA

SDS-PAGE was carried out on 1.5 mm NuPAGE NOVEXs 4–12% Bis-Tris Gels using NuPAGE MES SDS Running Buffer (20x stock) at 160 V for 1 h. Samples were incubated with NuPAGE LDS Sample Buffer with reducing agent according to the manufacturer's instructions (Invitrogen). Protein loading per lane was 1.8–2 μg with Precision Plus Protein™ Kaleidoscope™ pre-stained protein standards (10–250 kDa) used as a reference. Following electrophoretic separation, proteins were visualized using Coomassie staining, or transferred to immunoblotting membranes using an iBlot transfer apparatus (Invitrogen). PVDF membranes were then blocked with 1% (w/v) BSA in TBS with Tween 20 (TBST) for 1 h, and then incubated with an anti-3-nitroTyr pAb (#06-284, 1:3000 dilution) in blocking solution overnight at 4 °C. Membranes were rinsed three times for 10 min with TBST before incubation with an HRP-conjugated anti-rabbit IgG antibody (1:10000 dilution) for 1 h. Unbound antibody was removed by washing three times for 10 min with TBST, then immune complexes were detected using Western Lightning Plus ECL reagent. Images were acquired using a Sapphire Biomolecular Imager (Azure Biosystems). For ELISA, proteins were coated in high-binding 96-well plates (Greiner) at 4 °C overnight with 50 μL per well. Unbounded proteins were then removed by washing twice with PBS (pH 7.4), followed by blocking with 1% (w/v) BSA in PBS, and incubation with anti-6-nitroTrp mAb (clone 117C, 1:3000 dilution) or anti-diTyr mAb (clone 1C3, 1:3000 dilution) at 4 °C overnight. Plates were rinsed twice with PBS and incubated with IgG secondary antibodies at 21 °C for 1 h. After three washes with PBS, the plates were incubated with ABTS solution (2,2'-azinobis-3-ethylbenzothiazoline-6-sulfonic acid) and H_2O_2 (1000:1). Absorbance values were then determined at 405 nm using a Spectra Max® i3x microplate reader.

2.7. Mass spectrometry – amino acid analysis

Amino acids released from AN by acid hydrolysis was analyzed by mass spectrometry essentially as previously described by Gamon et al. [29]. Briefly, protein samples (25 μg) were precipitated with trichloroacetic acid (w/v 8 %) and spiked with stable isotope-labelled amino acid standards before drying down using a centrifugal vacuum concentrator for 30 min at 30 °C. The resulting pellet was hydrolyzed overnight in 4 M methanesulfonic acid with 0.2 % w/v tryptamine (50 μL) under vacuum at 110 °C. Amino acids were partially purified by solid-phase extraction using 30 mg/1 mL mixed-mode strong cation exchange Strata X–C cartridges (Phenomenex). Eluted fractions were dried at 30 °C under vacuum overnight, and then dissolved in 50 μL of 0.1 % formic acid. Analytes were quantified by ESI LC-MS in positive ion mode using a Bruker Impact HD II mass spectrometer. Samples were separated by gradient elution using an Imtakt Intrada Amino Acid 100 × 3.0 mm column with acetonitrile/formic acid (Solvent A; 100/0.3) and acetonitrile/100 mM ammonium formate (Solvent B; 20/80). MS analyses and quantification was performed at the MS^1 level.

2.8. Peptide mapping mass spectrometry

AN (25 μL, 5 μM) exposed to ONOOH as described above (section 2.3) was mixed with 75 μL 8 M urea (in 100 mM Tris, pH 8.0) and 1 μL LysC (20 ng μL^{-1}; Promega) then incubated at 21 °C for 4 h. Subsequently 150 μL 100 mM Tris (pH 8.0), 500 μL H_2O and 2 μL GluC (20 ng μL^{-1}; Promega) were added, and the samples incubated overnight at 21 °C. Following solid phase extraction with Stage-tips, samples were analyzed on a Bruker Impact II ESI-QTOF (Bruker Daltonics) mass spectrometer in the positive ion mode with a Captivespray ion source connected on-line to a Dionex Ultimate 3000RSnano chromatography systems (Thermo Fisher Scientific). Peptides were separated on a Bruker Nanoelute column (15 cm × 75 μm ID) with a solvent gradient over 65 min, using acetonitrile with 0.1% formic acid at a flow rate of 300 nL min^{-1}. The MS scan range was 150–1750 m/z with a cycle time of 2 s using MS and MS/MS sampling rates of 2 Hz. Database searches were performed with MaxQuant v1.6.1.0 using the following parameters: enzyme: GluC and LysC, with three missed cleavages; variable modification: Tyr and Trp nitration (+44.985 Da) and dinitration (89.97 Da); mass tolerance: 0.07 and 0.005 Da (first and main searches, respectively); MS/MS mass tolerance: 40 ppm (first and main searches).

2.9. Circular dichroism and thioflavin T binding

Circular dichroism (CD) spectra were acquired on a Jasco-815 CD Spectrometer (Jasco Corporation, Japan) and used to monitor the secondary structure of AN [30]. Far-UV CD spectra of AN (prepared as described in section 2.3), and diluted to 0.10 mg mL^{-1} (10.6 μM) with 10 mM phosphate buffer, pH 7.4, were recorded between 190–260 nm, in a 1-mm cell at 25 °C, at 1 nm intervals with a 1 nm bandwidth, and a scan speed of 50 nm min^{-1}, with six scans averaged for each spectrum. Reference samples without AN were measured correspondingly and subtracted using the Jasco Spectra Analysis software. The folding of AN was verified using the BeStSel online resource [31,32]. For CD measurement as a function of temperature (20–90 °C; 1 °C min^{-1}), the CD (at 227 nm) was measured in a 10-mm temperature-controlled cell with a 2 nm bandwidth. All CD data was converted to mean residue ellipticity using a molar concentration of 10.6 μM and 82 residues in AN (considering removal of the N-terminal methionine). The binding of Thioflavine T (ThT) was examined using protein solutions diluted to 10 μM with 10 mM phosphate buffer, pH 7.4, in the presence of 25 μM ThT and 20 μM 3-[(3-cholamidopropyl)dimethyl-ammonio]-1-propane sulfonate (CHAPS) and then analyzed in a Spectra Max® i3x microplate reader with λ_{ex} 440 nm (9 nm slit width) and emission recorded over the range 465–600 nm with a 15 nm slit width, with three spectra averaged.

2.10. Small-angle X-ray scattering

Small-angle X-ray scattering (SAXS) was carried out on oxidized AN samples (prepared as described in section 2.3), diluted to 100 μM with 10 mM phosphate buffer, pH 7.4. Measurements were performed on an optimized NanoSTAR SAXS instrument [33] from Bruker AXS, equipped with scatterless pinholes [34] and a liquid Ga metal jet X-ray source (Excillum) [35], with an acquisition time of 30 min at 20 °C. The data are presented as a function of the scattering vector q that is dependent on the scattering angle 2θ with $q = 4\pi/\lambda \sin\theta$, where $\lambda = 1.34$ Å. The SUPERSAXS program package (Oliveira, C.L.P. and Pedersen J.S, unpublished) was used for background subtraction and to convert data to

an absolute scale with water as a calibration standard. An indirect Fourier transformation was performed on the SAXS data [36,37] in order to obtain pair distance distribution functions ($p(r)$), with the latter being a histogram of distances between pairs of points, weighted by the excess scattering length density in these two points and thereby give structural information in real space. This can be used to determine the maximum diameter (D_{max}) of the particles, as well as shape information. The radius of gyration, R_g, and forward scattering, $I(0)$, was obtained for the complete unfolding series by performing Guinier fits. $I(0)$ is approximately proportional to the protein concentration and mass and can therefore be used to calculate the protein aggregation state. Molecular mass (Mm) was determined according to equation (1):

$$Mm = I(0) \cdot NA / (c \cdot \Delta\rho_m^2) \quad (1)$$

where c is the sample concentration, $\Delta\rho_m = 2.0 \times 10^{10}$ cm g^{-1} is the scattering length density difference per unit mass and NA is Avogadro's constant. The number of monomers in each sample was obtained using the theoretical molecular mass of AN (9.4 kDa).

2.11. Thermophoresis

AN prepared as described in section 2.3, was diluted to 1 mg mL^{-1} in 10 mM phosphate buffer and placed in standard glass capillaries. The samples were then analyzed in a nano differential scanning fluorimetry (nanoDSF) device (Prometheus NT.48; NanoTemper Technologies, Munich, Germany). The sample temperature was varied in a linear manner from 20 to 95 °C at a rate of 1 °C min^{-1}. After reaching the target temperature, the samples were cooled to 20 °C at the same rate. During the temperature scan, the retroreflective intensity of the light beam passing through the capillary was measured to detect protein aggregation. The scattering signal was normalized to a baseline signal to obtain a value defined as "excess scattering".

2.12. Statistics

Statistical analyses were performed using GraphPad Prism (version5.0, GraphPad Software, SanDiego, CA, USA) and IBM SPSS 22.0. One-way ANOVA with post hoc analysis using Tukey's multiple comparison test were performed on data from at least three independent experiments, with $p < 0.05$ considered significant, and the following annotation; *$p < 0.05$,**$p < 0.01$, ***$p < 0.001$, ****$p < 0.0001$.

3. Results

3.1. ONOOH and SIN-1 induce dose-dependent nitration of anastellin

AN (5 μM) was treated with bolus ONOOH at 1:1–1:100 molar ratios (protein:ONOOH), then analyzed by SDS-PAGE to assess changes in protein structure. Native AN appeared as a single monomer band on

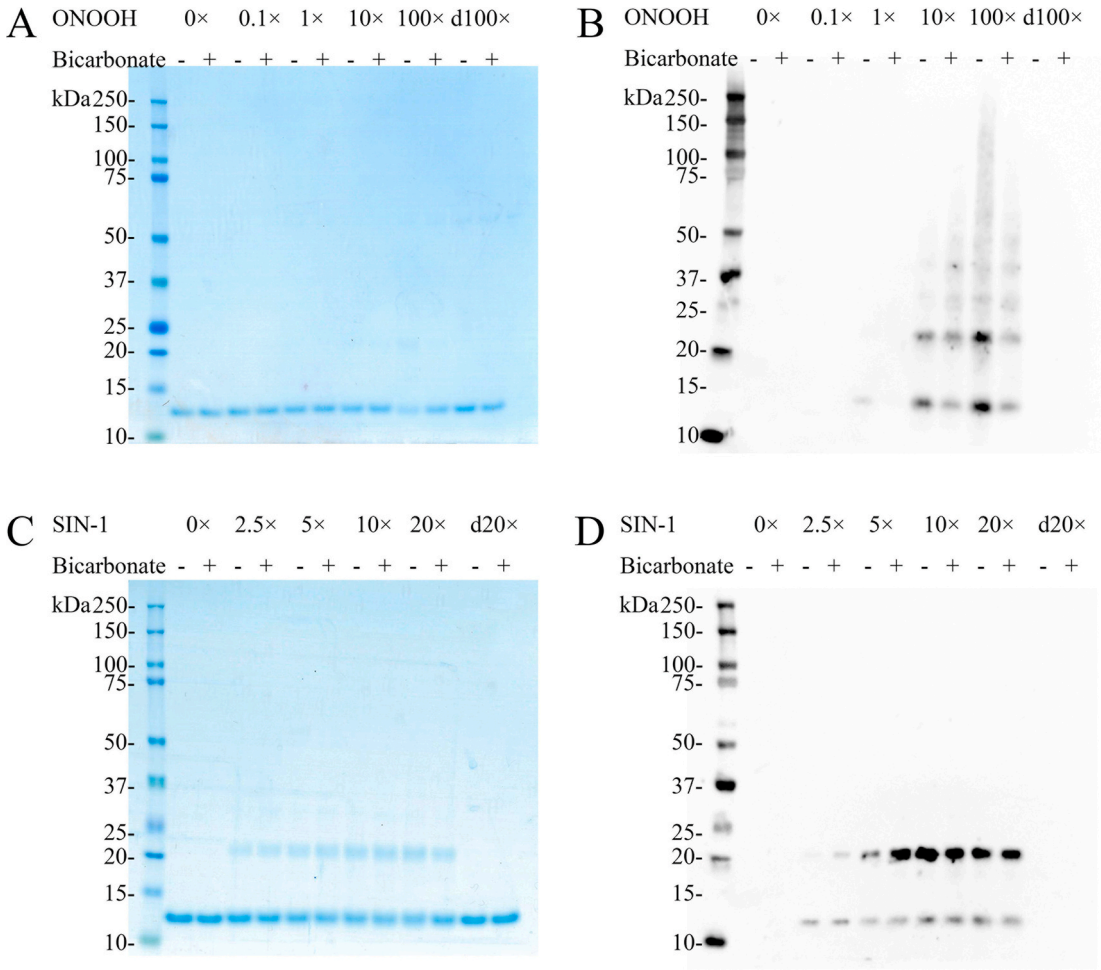

Fig. 1. Structural modifications to AN induced by ONOOH and SIN-1. Purified AN (5 μM, in 100 mM phosphate buffer, pH 7.4) was exposed to ONOOH (A and B) or SIN-1 (C and D) at the molar ratios indicated for 30 min at 37 °C, in either the absence (−) or presence (+) of 25 mM sodium bicarbonate ($NaHCO_3$) followed by separation by SDS-PAGE. Structural modifications were detected using either Coomassie staining (A and C), or by immunoblotting to PVDF membrane with subsequent probing for the presence of 3-nitroTyr (B and D). Molecular mass markers are shown for reference.

Coomassie-stained gels (Fig. 1A). The apparent molecular mass of the protein does not accurately match the expected mass of the protein, probably as a result of the presence of the His-tag which has been reported previously to result in abnormal gel migration [38]. The intensity of this band decreased with increasing oxidant exposure, with this being particularly noticeable at the highest oxidant doses (Fig. 1A); these changes were not observed with decomposed oxidant solutions. Corresponding immunoblots using a 3-nitroTyr antibody demonstrated a dose-dependent increase in 3-nitroTyr formation on AN with equimolar or greater levels of ONOOH (Fig. 1B). An increase in material with molecular mass $\geq$ 20 kDa was detected concurrently, consistent with the formation of dimeric and oligomeric species. These bands were apparent with a ten-fold excess of ONOOH (50 μM), and increased with higher excesses of oxidant (Fig. 1B). In the presence of $NaHCO_3$, the loss of the parent band was less pronounced, and lower levels of non-reducible high molecular mass species were detected. Less 3-nitroTyr was formed in the presence of $NaHCO_3$, consistent with the formation of peroxynitrosocarbonate ($ONOOCO_2^-$) [39].

AN was also exposed to SIN-1 (5-amino-3-(4-morpholinyl)-1,2,3-oxadiazolium chloride, also known as linsidomine) a compound that releases $O_2^{\cdot-}$ and $NO^{\cdot}$ with a 1:1 stoichiometry when dissolved in aqueous solution, generating a steady flux of $ONOO^-$/ONOOH [40]. Exposure to SIN-1 resulted in a dose-dependent increase in 3-nitroTyr formation and dimerization of AN, but in contrast to the bolus addition experiments with ONOOH, higher molecular mass species were not detected (Fig. 1C and D). The presence of $NaHCO_3$ did not significantly affect the modification of AN induced by SIN-1 as observed by SDS-PAGE, although a slight increase in 3-nitroTyr was seen at low doses of SIN-1.

Exposure of AN to increasing concentrations of ONOOH resulted in increased formation of di-Tyr and 6-nitroTrp, as detected by ELISA (Fig. 2). The maximum yield of di-Tyr was obtained with moderate excesses of oxidant; higher oxidant levels resulted in a reduced yield, possibly due to further reactions of this product (e.g. tri-tyrosine formation) (Fig. 2A). The formation of 6-nitroTrp in AN occurred in a dose-dependent manner with significantly elevated levels observed with 500 μM ONOOH (100-fold molar excess; Fig. 2B).

The concentrations of 3-nitroTyr, di-Tyr, and 6-nitroTrp, together with the corresponding parent amino acids Tyr and Trp, in AN exposed to ONOOH were evaluated by quantitative LC-MS following acid hydrolysis, and separation of released amino acids by liquid chromatography, as described in the Materials and methods. As reported previously [29], the parent amino acids were lost in a ONOOH dose-dependent manner (Fig. 3D and E), with this being matched by an corresponding increase in the yield of the modified species, particularly at low oxidant doses (Fig. 3A–C). With higher oxidant doses a plateau and subsequent decrease in the yield of di-Tyr were observed as seen in the ELISA experiments. The overall pattern of modified products observed by mass spectrometry and ELISA were however similar. The specific sites of modification on AN were examined by LC-MS/MS peptide mass mapping, after proteolytic digestion. In agreement with the results presented in Fig. 1–3, a dose-dependent increase in the number of identified nitrated peptides was observed, with each of the four Tyr and two Trp residues in AN detected as modified species (Table 1).

3.2. *Modified anastellin displays impaired capacity to polymerize fibronectin*

When AN is mixed with FN, insoluble fibrils (superfibronectin, sFN) are formed [8]. The kinetics of sFN formation with native or ONOOH–modified AN was monitored as turbidity at 550 nm after mixing AN with FN. At moderate ONOOH concentrations ($\leq$ 80 μM) the time course of sFN formation with modified AN was similar to the native protein, with an initial rapid increase in turbidity, followed by a slower phase (Fig. 4A). However, at the highest concentration of ONOOH (800 μM) there was a lag phase before the increase in turbidity was detected, consistent with a reduced ability of AN to polymerize FN (Fig. 4A). Conversely, the kinetic profiles of sFN formation using *native* AN mixed with either native or ONOOH-modified FN were similar, suggesting that modification of FN under these conditions does not influence the polymerization process (Fig. 4B).

sFN formation was also monitored using a sedimentation assay where insoluble fibrils formed on incubation of AN with FN, were isolated by centrifugation, and analyzed by SDS-PAGE. In agreement with the turbidity data (Fig. 4), high yields of sFN were obtained after mixing AN with FN, whereas only low levels of aggregates where observed with either protein in isolation (data not shown). The yield of sFN was quantified by comparing the intensities of the AN and FN monomer bands in insoluble sFN pellets formed after incubation of native FN with ONOOH-treated AN (Fig. 5A). For native FN incubated with ONOOH-treated AN, a dose-dependent decrease in the intensity of the AN monomer band was detected. This decrease might arise (at least partially) from ONOOH-induced oligomer formation from AN (Fig. 1). In contrast, the decreased intensity of the monomer band for FN (which had not been exposed to oxidant) in Fig. 5A is most likely due to reduced yields of sFN from ONOOH-modified AN, in accordance with the turbidity data (Fig. 4). Corresponding immunoblots provided evidence for a dose-dependent increase in 3-nitroTyr and oligomeric species in sFN formed with AN exposed to equimolar or greater levels of ONOOH, suggesting that modified AN can be incorporated into sFN (Fig. 5D). The intensity of the 3-nitroTyr signal decreased at higher levels of oxidant, which may be due to a decrease in the incorporation of modified AN into sFN, and/or a reduction of total yield of sFN.

Sedimentation assays were also performed with native AN and ONOOH-treated FN (Fig. 5B). The observed dose-dependent decrease in intensity of the FN monomer band in sFN from ONOOH-treated samples is likely to be due to the formation of higher molecular mass aggregates, as observed previously for FN exposed to ONOOH [41]. No significant decrease was however observed for the AN monomer band in sFN, formed after treatment of FN with ONOOH (Fig. 5B). These results suggest that oxidant exposure of FN does not influence the yield of sFN, under the conditions tested, in agreement with the turbidity data (Fig. 4). 3-NitroTyr and oligomeric species were detected on FN in sFN, with the level of these increasing at higher oxidant doses, suggesting that modified FN is incorporated into sFN (Fig. 5E). Incubation of

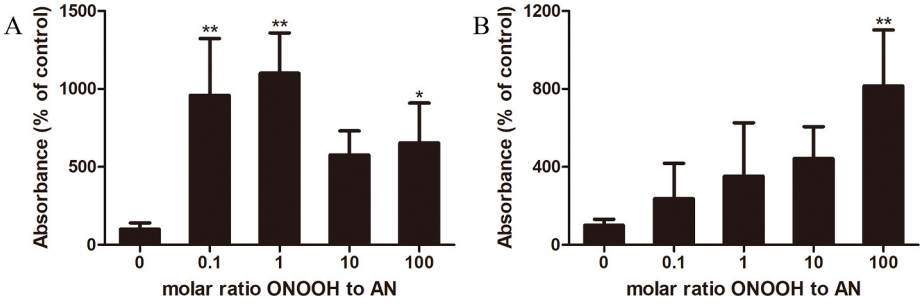

Fig. 2. Detection of di-Tyr (A) and 6-nitroTrp (B) on AN arising from exposure to ONOOH, as determined by ELISA. Purified AN (5 μM, in 100 mM phosphate buffer, pH 7.4) was exposed to ONOOH at the molar ratios indicated for 30 min at 21 °C. Modifications were quantified with ELISA using specific antibodies against di-Tyr (mAb clone 1C3) and 6-nitroTrp (mAb clone 117C). Statistical differences relative to control were analyzed by one-way ANOVA with Tukey's post-hoc test. Data are presented as means ± SD from three experiments, and are expressed as % values relative to those detected in the control without added ONOOH.

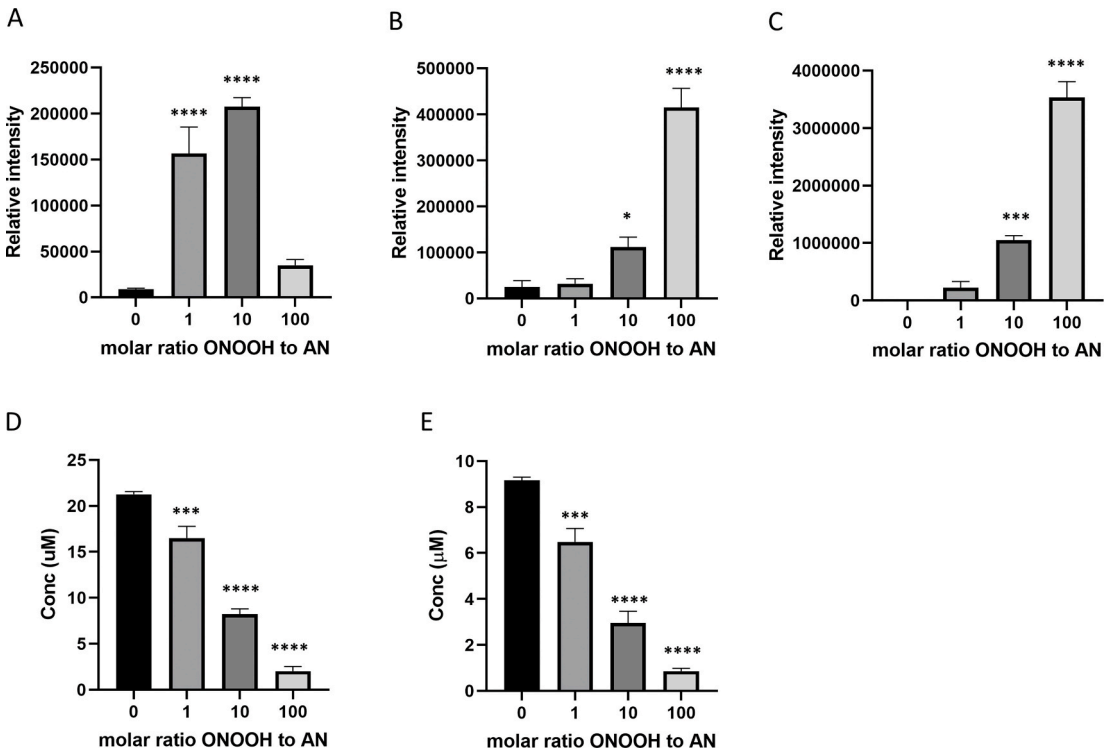

Fig. 3. Quantification of the modification products di-Tyr (A), 6-nitroTrp (B), 3-nitroTyr (C), and the parent amino acids Tyr (D), and Trp (E) in AN (5 μM) exposed to ONOOH (0–500 μM) by LC-MS analysis of free amino acids and product species after protein digestion using methanesulfonic acid (see Materials and methods). Statistical differences relative to the control without added ONOOH was determined by one-way ANOVA using Tukey's post-hoc test. Fig. 3D and E are reprinted from Ref. [17] with permission from Elsevier.

Table 1
Nitrated peptides from AN (5 μM) exposed to different concentrations of ONOOH detected by mass spectrometry following proteolytic digestion with LysC and GluC.

Sequence¤	Nitrated residues	ONOOH 0 μM	ONOOH 0.5 μM	ONOOH 5 μM	ONOOH 50 μM	ONOOH 500 μM
YILRWRPK	Tyr15			+	++	++
YILR**W**RPK	Tyr15, Trp19				++	++
YILR**W**RPK	Trp19			+		
NSVGR**W**KEATIPGHLNSYTIK	Trp28				+	
NSVGR**W**KEATIPGHLNS**Y**TIK	Trp28, Tyr40				+	++
NSVGR**W**KEATIPGHLNS**Y**TIK	Trp28, Tyr40					+
NSVGRWKEATIPGHLNS**Y**TIK	Tyr40		+	+		
EATIPGHLNS**Y**TIK	Tyr40			+	++	++
ATIPGHLNS**Y**TIK	Tyr40			+	+	+
GLKPGVV**Y**E	Tyr51			+	+	++
GLKPGVV**Y**E	Tyr51					++
GQLISIQQ**Y**GHQE	Tyr61			+	++	++
GQLISIQQ**Y**GHQE	Tyr61				+	+

¤ = 3-nitroTyr/6-nitroTrp residues are highlighted in bold. Residues modified by dinitration are underlined.
+ = detected in 1 replicate.
++ = detected in 2 replicates.

preformed sFN with ONOOH decreased the intensity of the monomer band of both AN and FN in a dose-dependent manner (Fig. 5C). 3-NitroTyr was however detected primarily on FN, when compared to AN (Fig. 5F). This is not unexpected given that FN is a much larger protein and has a greater number of ONOOH reactive side-chains. Thus FN contains 100 Tyr and 39 Trp residues, respectively (based on the canonical sequence of human FN, Uniprot ID P02751), whereas AN contains 4 Tyr and 2 Trp. Assuming a molar 4:1 AN:FN ratio in sFN as reported previously [11], this corresponds to an approximate 6- and 5-fold higher concentration of Tyr and Trp in FN, when compared with AN, under these conditions.

3.3. ONOOH induces aggregation of anastellin

As the data reported above indicate formation of AN oligomers on oxidant exposure, the size and shape of these species were examined in solution using SAXS. Fig. 6A shows normalized scattering data for AN solutions that had been exposed to different concentrations of ONOOH. These data indicate that there are no significant differences amongst the samples treated with low micromolar concentrations of ONOOH. However, for samples exposed to higher concentrations of ONOOH (≥ 800 μM), the intensity increased both in the low and the high q regions, indicating that the size of the AN species is increased. Fig. 6B shows the distance distribution function ($p(r)$) of the AN samples, which can be

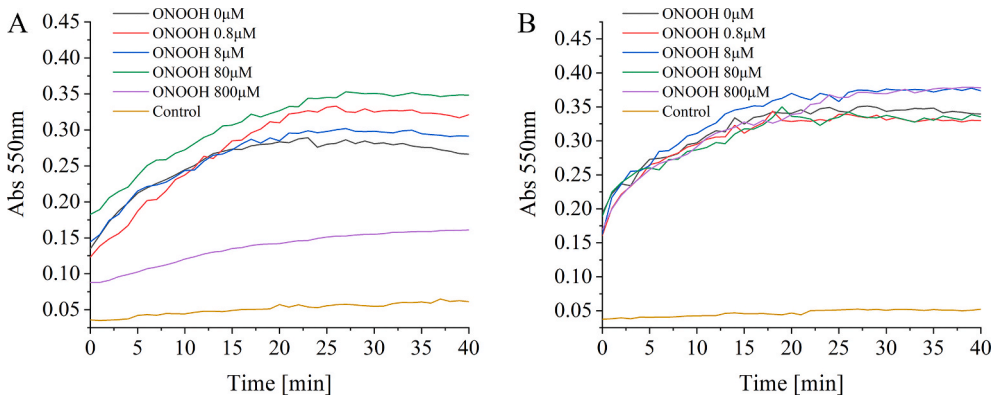

Fig. 4. Effect of ONOOH on kinetics of sFN aggregation. FN (1.4 μM) and AN (40 μM) were mixed in 10 mM phosphate buffer pH 7.4, with AN (A) or FN (B) exposed to the indicated concentrations of ONOOH for 30 min prior to buffer exchange into 10 mM phosphate buffer and mixing. The turbidity of the solution was then measured at 550 nm over 40 min at 21 °C. 10 mM phosphate buffer was used as control.

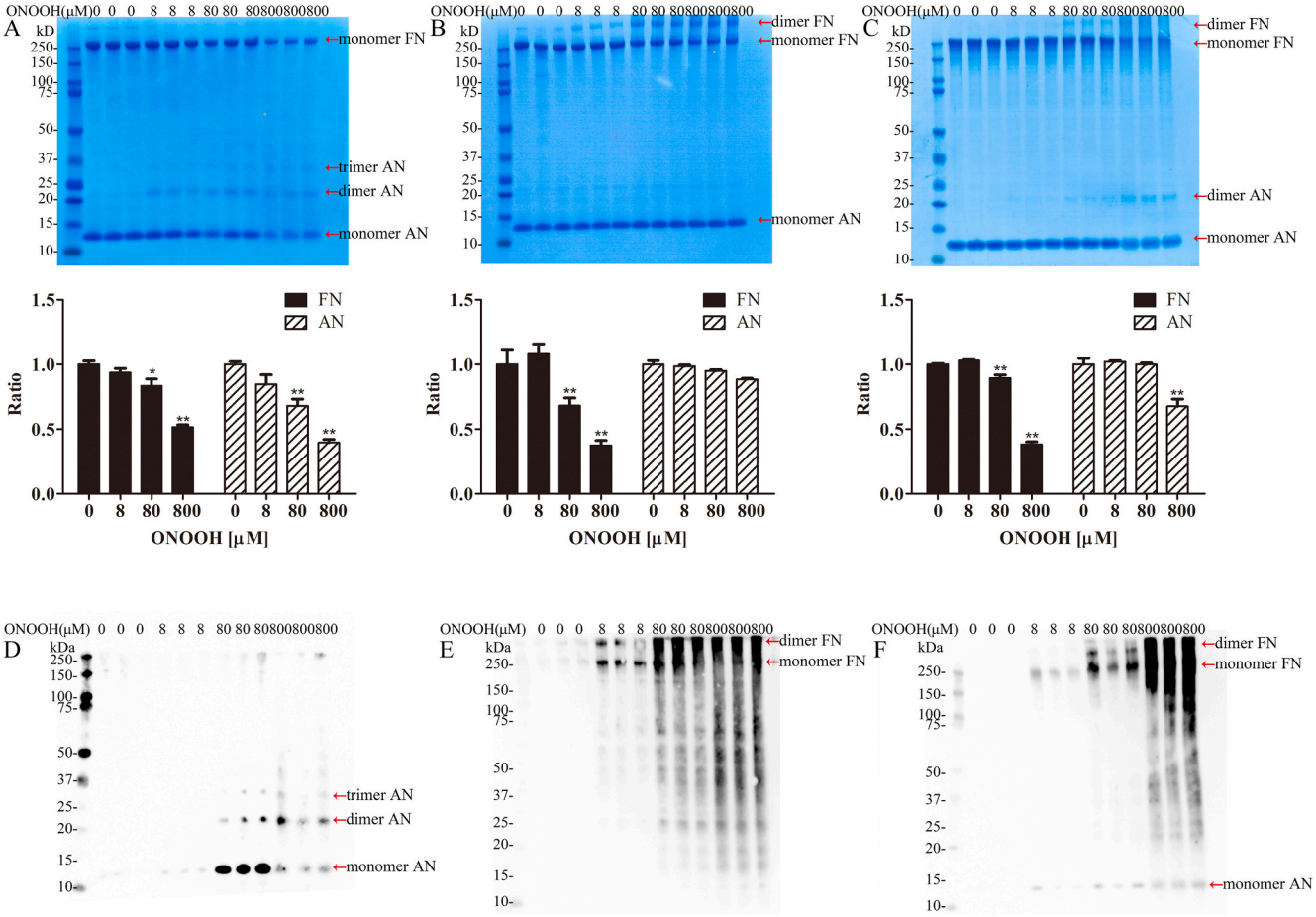

Fig. 5. Sedimentation assay of sFN formation from: native FN mixed with ONOOH-exposed AN (A, D); native AN mixed with ONOOH-exposed FN (B, E), and native FN and AN where the insoluble sFN pellet is exposed to ONOOH (C, F). AN and FN was incubated overnight at 21 °C, followed by centrifugation and washed pellets with insoluble fibrils were separated by SDS-PAGE under reducing conditions. The intensities of the Coomassie-stained monomer bands (indicated by arrows in the panels) were determined by image analysis, with these data presented below each gel in panels A–C. Data are presented as means ± SD from three experiments, and are expressed as a ratio relative to band intensity for the respective control data. Statistical differences relative to control without added ONOOH were assessed by one-way ANOVA with Tukey's post-hoc test. Panels D–E display the corresponding immunoblots probed for the presence of 3-nitroTyr.

used to determine the average molecular mass (Mm) and radius of gyration (R_g) of the particles. Based on these data, the Mm of native AN is predicted to be 12 kDa, about 1.3 times higher than the theoretical Mm of AN monomers (9.4 kDa), and consistent with the presence of mainly monomeric and dimeric species. Treatment of 40 μM AN with low micromolar concentrations of ONOOH, gave only modest increases in Mm (Table 2), whereas with 800 μM and 8 mM ONOOH, the average Mm for soluble AN species was 26.7 and 104.8 kDa, respectively, indicating the formation of large oligomers and aggregates; this is consistent with the SDS-PAGE and immunoblot data (Fig. 1). The R_g determined for native AN (approximately 1.9 nm) did not increase significantly with low micromolar ONOOH (Table 2), but this increased to 2.4 and 11.5 nm

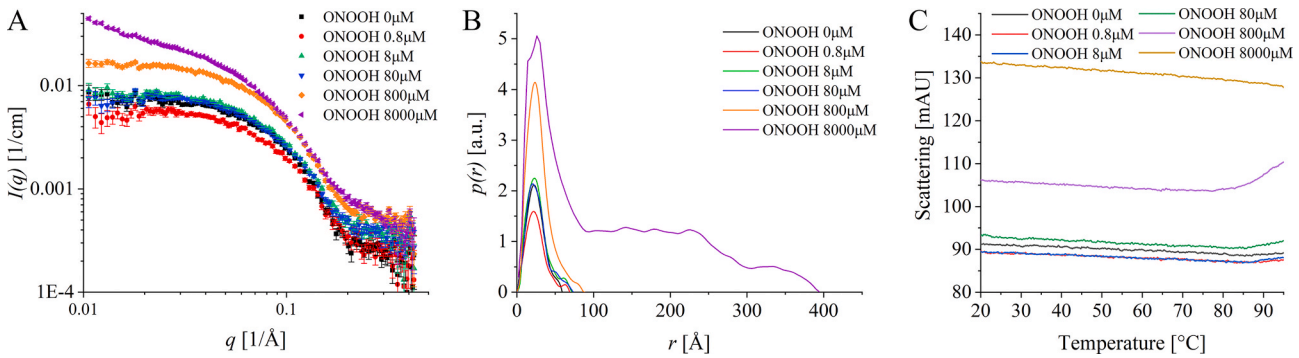

Fig. 6. Aggregation of AN (40 μM) treated with different concentrations of ONOOH (0.8 μM−8 mM) for 30 min at 20 °C, analyzed by: (A, B) SAXS, and (C) nanoDSF coupled with thermal denaturation from 20 to 95 °C. (A) Variation of the scattered intensity $I(q)$ versus the momentum transfer $q = 4\pi/\lambda \sin\theta$. (B) The pair distance distribution functions ($p(r)$) was obtained from the indirect Fourier transformation of the intensities (see main text and Materials and methods).

Table 2
Determination of molecular mass (Mm) and gyration radius (R_g) for AN (40 μM) exposed to ONOOH by SAXS analysis. Physical parameters are determined from pair distance distribution functions ($p(r)$). The radius of gyration, R_g, and forward scattering, $I(0)$, was obtained for the complete unfolding series by performing Guinier fits. The average number of monomers in each species was estimated based on the theoretical molecular mass for AN (9.4 kDa).

	Concentration (mg ml^{-1})	$I(0)$ (cm^{-1})	Mm (kDa)	Number of monomers	R_g (nm)
ONOOH 0 μM	0.925	0.007	12.0 ± 0.1	~1.3	1.9 ± 0.1
ONOOH 0.8 μM	0.74	0.006	11.8 ± 0.1	~1.3	1.9 ± 0.1
ONOOH 8 μM	0.925	0.009	13.9 ± 0.1	~1.5	2.0 ± 0.1
ONOOH 80 μM	0.74	0.008	16.5 ± 0.2	~1.8	2.0 ± 0.1
ONOOH 800 μM	0.925	0.016	26.7 ± 0.3	~2.8	2.4 ± 0.1
ONOOH 8000 μM	0.925	0.064	104.8 ± 1.5	~11.2	11.5 ± 0.1

with 800 μM and 8 mM ONOOH, respectively, in agreement with the Mm data (Table 2).

AN aggregation was also studied by measuring light scattering in a nanoDSF device coupled with thermal denaturation. In agreement with the SAXS data, a significant increase in light scattering was detected for the samples treated with ONOOH, consistent with a dose-dependent increase in aggregate formation (Fig. 6C). A further increase in light scattering above 80 °C was observed for AN treated with 800 μM ONOOH.

3.4. Modified anastellin displays decreased thermal stability

The data reported above indicate that major structural perturbations occur on AN with extensive modification by ONOOH. The secondary structure of the protein was therefore investigated by far-UV CD spectroscopy. In agreement with previous observations [42] native AN displays a spectrum with a maximum at 198 nm and minimum at 228 nm (Fig. 7A), characteristic of the beta-sheet sandwich structures of FNIII modules. The observed CD is consistent with solution NMR data and indicate approximately 30% anti-parallel beta-sheets, 10% turns and 60% unordered structural elements, when analyzed with the BeStSel algorithm [31,32,42]. These spectral features were retained when AN (40 μM) was treated with low or moderate levels of ONOOH, whereas treatment with 4–8 mM ONOOH (100 or 200-fold molar excesses) gave rise to features consistent with a largely disordered conformation, and minima at about 202 nm. This loss of folding after ONOOH treatment could be caused by a disruption of the hydrophobic core as two of the Tyr residues and both the Trp residues are proximal to the beta-sheet content of AN. The impact of ONOOH on thermal stability of AN was also monitored by CD. As the sample temperature was increased, the CD signal of AN at 227 nm decreased, passing through a thermal transition interval leading to conversion to a random coil structure (Fig. 7B). It has previously been reported that aromatic residues may influence CD signals in the 220–230 nm region [43]. However, at 227 nm the main contribution to the CD appears to come from the amide backbone transitions, as determined by BeStSel analysis [31,32] (see Materials and Methods) demonstrating that it is not necessary to take aromatic contributions into account when analyzing the far-UV CD spectrum. The changes in CD with temperature reflect both changes in protein folding as well as effects of a linear temperature-dependence of the CD of a given fold [44]. Untreated AN exhibited a sharp thermal transition with a T_m

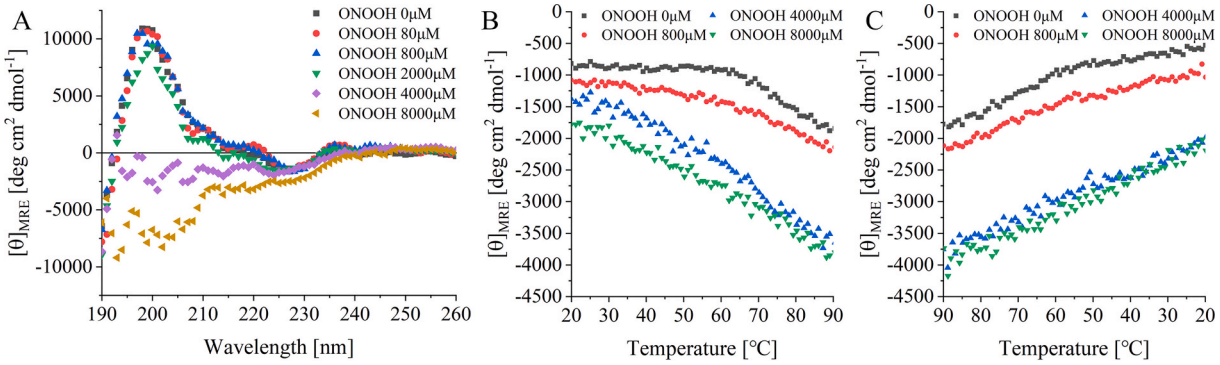

Fig. 7. AN (40 μM) was treated with different concentrations of ONOOH (0.8 μM−8 mM) for 30 min at 20 °C, then analyzed using far-UV CD spectroscopy. (A) CD spectra over the wavelength range 190–260 nm. (B, C) Profiles of thermal denaturation (B) and refolding (C) were detected by far-UV CD spectra at 227 nm in a 10-mm cell with the temperature increased at a rate of 1 °C min^{-1} (B), and then subsequently decreased (C).

of ~65 °C. When the sample was cooled down, the CD gradually increased without abrupt changes, consistent with refolding and reversible thermal denaturation of AN (Fig. 7C), in agreement with previous data from $FNIII_1$ modules [45]. After treatment with a 20-fold molar excess of ONOOH (800 μM), the thermal stability of AN was altered as indicated by a much broader thermal transition and a slightly decreased T_m. With higher ONOOH concentrations the existence of a largely disordered conformation at room temperature prevented estimation of T_m values.

The benzothiazole dye ThT, which displays enhanced fluorescence when it binds to beta sheet-rich structures in amyloids, is widely used as a probe for protein unfolding and aggregation [46–48]. Native AN showed a high fluorescence emission intensity at 495 nm consistent with ThT binding, and the presence of hydrophobic patches and a beta-sheet structure on the protein surface (Fig. 8). The intensity of this fluorescence decreased upon ONOOH exposure in a dose-dependent manner, consistent with the loss of these structural elements. This may also be due to the conversion of the Tyr and Trp residues to more hydrophilic or charged products (see Discussion). Furthermore, this behavior suggests that the aggregates formed at high ONOOH concentrations have non-amyloid structures.

4. Discussion

This study demonstrates that ONOOH exposure impairs the ability of AN to initiate formation of sFN fibrils. This loss-of-function is associated with dramatic changes to the structure of AN with the formation of oligomers and aggregates. Significant levels of 3-nitroTyr and 6-nitroTrp were generated from Tyr and Trp residues, and the sites of these specific modifications have been identified. These data are consistent with previous reports demonstrating significant ONOOH-mediated damage at these side-chains [49]. Formation of di-Tyr cross-links was also detected although a decrease in the formation of these cross-links were observed at the highest ONOOH concentrations examined. This decrease in detected di-Tyr, may possibly be due to extensive aggregation and protein precipitation, which in the case of ELISA-based analyses may prevent access of the antibody to particular sites, or may be as a result of further oxidation (e.g. to tri-tyrosine). Consistent with the formation of di-Tyr, an increased detection of species with apparent molecular mass of approximately 20 kDa, and also higher mass species, were detected with ONOOH concentrations >50 μM, presumably corresponding to cross-linked dimers and higher oligomers of AN. Cys, cystine and Met residues are known to be major protein targets for ONOOH (with this occurring via both one- and two-electron oxidation reactions) [25].

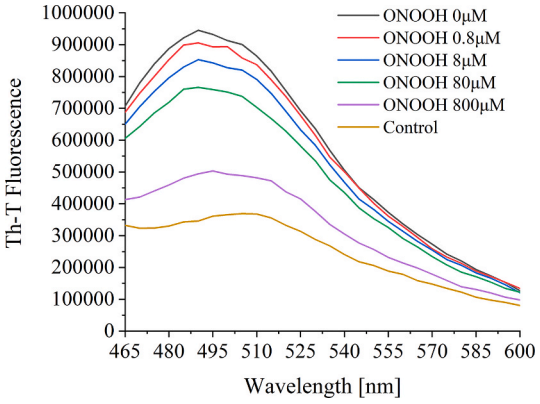

Fig. 8. Binding of ThT to modified AN. AN (40 μM) was incubated with different concentrations of ONOOH (0.8 μM–8 mM) for 30 min, with the binding of ThT (25 μM) subsequently examined by fluorimetry with λ_{ex} 440 nm (9 nm slit width) and λ_{em} 465–600 nm (15 nm slit width) using 10 μM AN in 10 mM phosphate buffer supplemented with 20 μM CHAPS. The control spectrum is that of ThT in the same buffer in the absence of AN.

However, these residues are absent in AN, and therefore Tyr and Trp residues are likely to be the major sites of modification with these reactions occurring via radical-mediated reactions. Consistent with this hypothesis, high levels of 3-nitroTyr were detected on the monomer, dimeric and oligomeric AN species. Evidence has also been obtained for the formation of significant concentrations of 6-nitroTrp from Trp residues. The formation of 3-nitroTyr and di-Tyr may reflect two alternative pathways for Tyr-derived phenoxyl radicals ($TyrO^{\cdot}$) formed on AN by $HO^{\bullet}$ and $NO_2^{\bullet}$ arising from decay of ONOOH, with the $TyrO^{\cdot}$ either undergoing dimerization to give di-Tyr, or further reaction with $NO_2^{\cdot}$ to give 3-nitroTyr. Similar reactions involving Trp-derived indolyl radicals ($TrpN^{\cdot}$) are believed to be responsible for the formation of 6-nitroTrp, via reaction of $TrpN^{\cdot}$ with $NO_2^{\bullet}$. Formation of the dimeric species, di-Trp, and also crossed-dimers (i.e. Trp-Tyr) may also occur; such species have been detected in other systems [50,51], and may also be formed with AN.

The presence of HCO_3^- decreased the observed extent of damage induced by bolus addition of ONOOH to AN solutions, in agreement with previous work on other ECM proteins such as laminin and FN [22,41,52]. $ONOO^-$ reacts with CO_2/HCO_3^- to form peroxynitrosocarbonate ($ONOOCO_2^-$) [53–55], which decomposes to form $NO_2^{\bullet}$and $CO_3^{\cdot-}$, so one potential explanation for this protection is the difference in reactivity of $HO^{\bullet}$ and $CO_3^{\cdot-}$, as the latter is less reactive than the former [56,57]. In contrast, HCO_3^- did not appear to have a protective effect toward modification of AN induced by treatment with SIN-1, which has been reported to form low fluxes of ONOOH in a sustained manner [40,58]. On the contrary, a slight increase in 3-nitroTyr formation was detected in the presence of HCO_3^- at low concentrations of SIN-1. It is therefore postulated that the influence of HCO_3^- on the reactivity of SIN-1 derived species towards AN is related to the overall flux of radicals (e.g. the kinetics of radical formation from $ONOOCO_2^-$ and ONOOH, and possible modulation of SIN-1 decomposition by HCO_3^-), and/or the occurrence of alternative reactions of the initial radicals formed from SIN-1 ($O_2^{\cdot-}$ and $NO^{\cdot}$).

ONOOH has been shown to induce changes in the secondary, tertiary, and quaternary structure of many proteins, including low-density lipoproteins, α-synuclein and cytochrome c [59–61]. The data presented here demonstrate that, although modifications occur at individual Tyr and Trp residues in AN in a facile manner, and are formed with even equimolar amounts of ONOOH (i.e. single hits per protein molecule), the β-strand fold of AN is rather resilient towards ONOOH-mediated structural changes, with no significant perturbations in the secondary structure observed with micromolar levels of ONOOH. However, with higher doses (>100 times molar excess; low millimolar ONOOH levels), AN undergoes unfolding, and the thermal stability of the protein is decreased. Aggregated species were also detected under these conditions, presumably stabilized by intermolecular interactions between unfolded species. However, aggregates were also observed after exposure to sub-millimolar levels of ONOOH, where the secondary structure of AN appears to be intact, suggesting that other mechanisms are also involved.

AN, which lacks the two β-strands that are present at the N-terminus of the full-length $FNIII_1$ module, has a flexible structure with exposed hydrophobic patches similar to those detected in the precursors of amyloid fibrils [42,62]. These patches are likely to be involved in sFN formation, but may also stabilize AN aggregates through intermolecular beta-strands, consistent with our observation that (unmodified) AN forms a complex with the dye ThT, a molecule that is known to bind to amyloid-type aggregates. Amyloid-like aggregates have also been reported to be formed from other FNIII modules, and also intact FN [63,64]. It was therefore relevant to investigate if these types of protein aggregates were also present in modified AN. However, ONOOH exposure did not increase binding of ThT to AN. On the contrary, a marked drop in ThT fluorescence was observed after exposure to high micromolar levels of oxidant, suggesting that the oxidation-induced aggregates are not stabilized by intermolecular beta-strands. This decreased

binding of ThT can also be rationalized in terms of the known properties of native and modified Tyr and Trp residues. Thus, the native amino acid side-chains are hydrophobic in nature and would be expected to associate with ThT, whereas the products 3-nitroTyr and 6-nitroTrp are more polar due to the presence of the nitro function. Furthermore, it is known that nitration of Tyr decreases the pK_a of the phenol function (Tyr-OH), present on the aromatic ring, from 10.5 to approximately 7.1 [65], such that at pH 7.4, a large proportion of the 3-nitroTyr will be present as the charged phenolate form (i.e. Tyr-O^-). The latter would not be expected to bind ThT. Moreover, such species may potentially stabilize high mass aggregates through intermolecular interactions with positive charges on the side-chains of lysine and arginine.

FN fibrils in the ECM are critical for adhesion, migration and proliferation of fibroblast, endothelial and epithelial cells and are also important for wound repair, including within the artery wall and skin [3, 66]. It has been proposed that native ECM assembly involves the transient unfolding of FNIII modules by mechanical forces induced through ECM-cell contacts between FN, integrin and actin. These FNIII modules promote the formation of fibrils through interactions between cryptic FN-FN interaction sites exposed by the strain-induced unfolding. This model is similar to the mechanism of sFN formation where hydrophobic patches in AN, which are exposed due to the absence of two beta-strands in the FNIII fold, are proposed to initiate fibrillation through interactions with transiently unfolded FNIII modules [11]. Thus, AN-promoted FN fibrillation can be regarded as a model of *in vivo* FN polymerization.

We have shown here that the ability of AN to polymerize FN is impaired with moderate ONOOH exposure, as indicated by the decreased yield of sFN in sedimentation assays. The lag phase observed in the turbidity assay with high ONOOH levels suggests that the kinetics of sFN formation are also affected. This would suggest that oxidant exposure modifies sites on AN that are important for FN polymerization. One candidate is Tyr40, which has been previously reported to be crucial for AN-induced sFN polymerization [42], and which we have demonstrated to be nitrated on ONOOH exposure. However, possible roles for other Tyr and Trp residues, which were also detected as modified species (nitrated or as dimers), cannot be excluded, so it is not currently possible to correlate the loss-of-function with modification at a particular residue, and it is probable that alterations at multiple residues may contribute. Even though ONOOH impairs the ability of AN to form sFN, modified AN species appear to be incorporated into sFN, as demonstrated by the detection of AN oligomers and 3-nitroTyr species in sFN. Similarly, modified FN molecules appear to be incorporated into sFN. In contrast to AN however, ONOOH treatment of FN does not appear to influence sFN polymerization under the conditions tested here. As discussed above, the extent of modification at particular sites on FN are likely to be lower than at specific residues in AN, due to the large number of other potentially reactive residues in FN which include reactive Cys, cystine, and Met residues, as well as large numbers of Tyr and Trp side chains.

Overall, the data presented here demonstrate that AN is readily modified by ONOOH with the level of structural perturbations increasing in a dose-dependent manner with higher oxidant concentrations, both at the level of individual side chains, as well as the overall protein structure, with this being associated with the formation of high molecular mass aggregates; the later may involve both covalently and non-covalently bound species. Further studies are however required to determine the role of individual modifications (e.g. at Tyr40), to investigate how oxidants influence the molecular interactions between AN and FN, and the consequences of these processes for sFN formation.

Declarations of Competing interestCOI

None.

Acknowledgements

This work was supported by the Novo Nordisk Foundation (Laureate grant: NNF13OC0004294 to MJD), the Danish Council for Independent Research | Natural Sciences (DFF-7014-00047 to MJD), and the China Scholarship Council (scholarship to Jianfei He). NanoTemper Technologies are acknowledged for providing access to nanoDSF instrumentation. We are grateful to Jan Skov Pedersen for access to the SAXS machine.

Appendix A. Supplementary data

Supplementary data to this article can be found online at https://doi.org/10.1016/j.redox.2020.101631.

References

[1] R.O. Hynes, Fibronectins, Springer, Verlag, 1990.
[2] R. Hynes, Molecular biology of fibronectin, Annu. Rev. Cell Biol. 1 (1) (1985) 67–90.
[3] W.S. To, K.S. Midwood, Plasma and cellular fibronectin: distinct and independent functions during tissue repair, Fibrogenesis Tissue Repair 4 (1) (2011) 21.
[4] A.J. Zollinger, M.L. Smith, Fibronectin, the extracellular glue, Matrix Biol. 60 (2017) 27–37.
[5] J.E. Schwarzbauer, D.W. DeSimone, Fibronectins, their fibrillogenesis, and in vivo functions, Cold Spring Harb, Perspect. Biol. 3 (7) (2011) a005041.
[6] Y. Mao, J.E. Schwarzbauer, Fibronectin fibrillogenesis, a cell-mediated matrix assembly process, Matrix Biol. 24 (6) (2005) 389–399.
[7] P. Singh, C. Carraher, J.E. Schwarzbauer, Assembly of fibronectin extracellular matrix, Annu. Rev. Cell Dev. Biol. 26 (2010) 397–419.
[8] A. Morla, Z. Zhang, E. Ruoslahti, Superfibronectin is a functionally distinct form of fibronectin, Nature 367 (1994) 193–196.
[9] J.M. Stine, G.J. Ahl, C. Schlenker, D.-V. Rusnac, K.r Briknarová, The interaction between the third type III domain from fibronectin and anastellin involves β-strand exchange, Biochemistry 56 (35) (2017) 4667–4675.
[10] T. Ohashi, A.M. Augustus, H.P. Erickson, Transient opening of fibronectin type III (FNIII) domains: the interaction of the third FNIII domain of FN with anastellin, Biochemistry 48 (19) (2009) 4189–4197.
[11] T. Ohashi, H.P. Erickson, Domain unfolding plays a role in superfibronectin formation, J. Biol. Chem. 280 (47) (2005) 39143–39151.
[12] A. Ambesi, P.J. McKeown-Longo, Conformational remodeling of the fibronectin matrix selectively regulates VEGF signaling, J. Cell Sci. 127 (17) (2014) 3805–3816.
[13] R.M. Klein, M. Zheng, A. Ambesi, L. Van De Water, P.J. McKeown-Longo, Stimulation of extracellular matrix remodeling by the first type III repeat in fibronectin, J. Cell Sci. 116 (22) (2003) 4663–4674.
[14] S. Bourdoulous, G. Orend, D.A. MacKenna, R. Pasqualini, E. Ruoslahti, Fibronectin matrix regulates activation of RHO and CDC42 GTPases and cell cycle progression, J. Cell Biol. 143 (1) (1998) 267–276.
[15] A. Ambesi, P.J. McKeown-Longo, Anastellin, the angiostatic fibronectin peptide, is a selective inhibitor of lysophospholipid signaling, Mol. Canc. Res. 7 (2) (2009) 255–265.
[16] R. You, R.M. Klein, M. Zheng, P.J. McKeown-Longo, Regulation of p38 MAP kinase by anastellin is independent of anastellin's effect on matrix fibronectin, Matrix Biol. 28 (2) (2009) 101–109.
[17] A. Ambesi, R.M. Klein, K.M. Pumiglia, P.J. McKeown-Longo, Anastellin, a fragment of the first type III repeat of fibronectin, inhibits extracellular signal-regulated kinase and causes G1 arrest in human microvessel endothelial cells, Canc. Res. 65 (1) (2005) 148–156.
[18] R. Pasqualini, S. Bourdoulous, E. Koivunen, V.L. Woods, E. Ruoslahti, A polymeric form of fibronectin has antimetastatic effects against multiple tumor types, Net. Med 2 (11) (1996) 1197–1203.
[19] M. Yi, E. Ruoslahti, A fibronectin fragment inhibits tumor growth, angiogenesis, and metastasis, in: Proc. Natl. Acad. Sci. U. S. A, vol. 98, 2001, 2.
[20] D.C. Hocking, K. Kowalski, A cryptic fragment from fibronectin's III1 module localizes to lipid rafts and stimulates cell growth and contractility, J. Cell Biol. 158 (1) (2002) 175–184.
[21] Y. Xia, J.L. Zweier, Superoxide and peroxynitrite generation from inducible nitric oxide synthase in macrophages, in: Proc. Natl. Acad. Sci. U. S. A, vol. 94, 1997, pp. 6954–6958, 13.
[22] G. Degendorfer, C.Y. Chuang, A. Hammer, E. Malle, M.J. Davies, Peroxynitrous acid induces structural and functional modifications to basement membranes and its key component, laminin, Free Radic. Biol. Med. 89 (2015) 721–733.
[23] S. Vanichkitrungruang, C.Y. Chuang, C.L. Hawkins, A. Hammer, G. Hoefler, E. Malle, M.J. Davies, Oxidation of human plasma fibronectin by inflammatory oxidants perturbs endothelial cell function, Free Radic. Biol. Med. 136 (2019) 118–134.
[24] R. Radi, G. Peluffo, M.a.N. Alvarez, M. Naviliat, A. Cayota, Unraveling peroxynitrite formation in biological systems, Free Radic. Biol. Med. 30 (5) (2001) 463–488.

[25] G. Ferrer-Sueta, N. Campolo, M. Trujillo, S. Bartesaghi, S. Carballal, N. Romero, B. Alvarez, R. Radi, Biochemistry of peroxynitrite and protein tyrosine nitration, Chem. Rev. 118 (3) (2018) 1338–1408.
[26] B. Halliwell, J.M.C. Gutteridge. Free Radicals in Biology and Medicine, Oxford University Press, Oxford, 2015.
[27] R.M. Uppu, W.A. Pryor, Synthesis of peroxynitrite in a two-phase system using isoamyl nitrite and hydrogen peroxide, Anal. Biochem. 236 (2) (1996) 242–249.
[28] D.S. Bohle, B. Hansert, S.C. Paulson, B.D. Smith, Biomimetic synthesis of the putative cytotoxin peroxynitrite, ONOO-, and its characterization as a tetramethylammonium salt, J. Am. Chem. Soc. 116 (16) (1994) 7423–7424.
[29] L.F. Gamon, C. Guo, J. He, P.M. Hägglund, C.L. Hawkins, M.J. Davies, Absolute quantitative analysis of intact and oxidized amino acids by LC-MS without prior derivatization, Redox Biol. 36 (2020), 101586. In press.
[30] N.J. Greenfield, Applications of circular dichroism in protein and peptide analysis, Trends Anal. Chem. 18 (4) (1999) 236–244.
[31] A. Micsonai, F. Wien, E. Bulyaki, J. Kun, E. Moussong, Y.H. Lee, Y. Goto, M. Refregiers, J. Kardos, BeStSel: a web server for accurate protein secondary structure prediction and fold recognition from the circular dichroism spectra, Nucleic Acids Res. 46 (W1) (2018) W315–W322.
[32] A. Micsonai, F. Wien, L. Kernya, Y.H. Lee, Y. Goto, M. Refregiers, J. Kardos, Accurate secondary structure prediction and fold recognition for circular dichroism spectroscopy, in: Proc. Natl. Acad. Sci. U. S. A, vol. 112, 2015, pp. E3095–E3103, 24.
[33] J.S. Pedersen, A flux-and background-optimized version of the NanoSTAR small-angle X-ray scattering camera for solution scattering, J. Appl. Crystallogr. 37 (3) (2004) 369–380.
[34] Y. Li, R. Beck, T. Huang, M.C. Choi, M. Divinagracia, Scatterless hybrid metal–single-crystal slit for small-angle X-ray scattering and high-resolution X-ray diffraction, J. Appl. Crystallogr. 41 (6) (2008) 1134–1139.
[35] A. Schwamberger, B. De Roo, D. Jacob, L. Dillemans, L. Bruegemann, J.W. Seo, J.-P. Locquet, Combining SAXS and DLS for simultaneous measurements and time-resolved monitoring of nanoparticle synthesis, Nucl, Instrum. Meth., B 343 (2015) 116–122.
[36] O. Glatter, A new method for the evaluation of small-angle scattering data, J. Appl. Crystallogr. 10 (5) (1977) 415–421.
[37] J.S. Pedersen, S. Hansen, R. Bauer, The aggregation behavior of zinc-free insulin studied by small-angle neutron scattering, Eur. Biophys. J. 22 (6) (1994) 379–389.
[38] R.M. Shelake, Y. Ito, J. Masumoto, E.H. Morita, H. Hayashi, A novel mechanism of "metal gel-shift" by histidine-rich Ni2+-binding Hpn protein from Helicobacter pylori strain SS1, PloS One 12 (2) (2017) e0172182.
[39] W.A. Pryor, J.-n Lemercier, H. Zhang, R.M. Uppu, G.L. Squadrito, The catalytic role of carbon dioxide in the decomposition of peroxynitrite, Free Radic. Biol. Med. 23 (2) (1997) 331–338.
[40] R.J. Singh, N. Hogg, J. Joseph, E. Konorev, B. Kalyanaraman, The peroxynitrite generator, SIN-1, becomes a nitric oxide donor in the presence of electron acceptors, Arch. Biochem. Biophys. 361 (2) (1999) 331–339.
[41] G. Degendorfer, C.Y. Chuang, H. Kawasaki, A. Hammer, E. Malle, F. Yamakura, M. J. Davies, Peroxynitrite-mediated oxidation of plasma fibronectin, Free Radic. Biol. Med. 97 (2016) 602–615.
[42] K. Briknarová, M.E. Åkerman, D.W. Hoyt, E. Ruoslahti, K.R. Ely, Anastellin, an FN3 fragment with fibronectin polymerization activity, resembles amyloid fibril precursors, J. Mol. Biol. 332 (1) (2003) 205–215.
[43] R.W. Woody, Contributions of tryptophan side chains to the far-ultraviolet circular dichroism of proteins, Eur. Biophys. J. 23 (4) (1994) 253–262.
[44] N.J. Greenfield, Using circular dichroism collected as a function of temperature to determine the thermodynamics of protein unfolding and binding interactions, Nat. Protoc. 1 (6) (2006) 2527–2535.
[45] S.V. Litvinovich, V.V. Novokhatny, S.A. Brew, K.C. Ingham, Reversible unfolding of an isolated heparin and DNA binding fragment, the first type III module from fibronectin, Biochim. Biophys. Acta 1119 (1) (1992) 57–62.
[46] B. Demeule, R. Gurny, T. Arvinte, Detection and characterization of protein aggregates by fluorescence microscopy, Int. J. Pharm. 329 (1–2) (2007) 37–45.
[47] H. Levine III, Thioflavine T interaction with synthetic Alzheimer's disease β-amyloid peptides: detection of amyloid aggregation in solution, Protein Sci. 2 (3) (1993) 404–410.
[48] P. Marinelli, S. Navarro, R. Graña-Montes, M. Bañó-Polo, M.R. Fernández, E. Papaleo, S. Ventura, A single cysteine post-translational oxidation suffices to compromise globular proteins kinetic stability and promote amyloid formation, Redox Biol. 14 (2018) 566–575.
[49] B. Alvarez, R. Radi, Peroxynitrite reactivity with amino acids and proteins, Amino Acids 25 (3–4) (2003) 295–311.
[50] L. Carroll, D.I. Pattison, J.B. Davies, R.F. Anderson, C. Lopez-Alarcon, M.J. Davies, Formation and detection of oxidant-generated tryptophan dimers in peptides and proteins, Free Radic. Biol. Med. 113 (2017) 132–142.
[51] G. Degendorfer, C.Y. Chuang, M. Mariotti, A. Hammer, G. Hoefler, P. Hägglund, E. Malle, S.G. Wise, M.J. Davies, Exposure of tropoelastin to peroxynitrous acid gives high yields of nitrated tyrosine residues, di-tyrosine cross-links and altered protein structure and function, Free Radic. Biol. Med. 115 (2018) 219–231.
[52] L.G. Lorentzen, C.Y. Chuang, A. Rogowska-Wrzesinska, M.J. Davies, Identification and quantification of sites of nitration and oxidation in the key matrix protein laminin and the structural consequences of these modifications, Redox Biol. 24 (2019) 101226.
[53] G.L. Squadrito, W.A. Pryor, Oxidative chemistry of nitric oxide: the roles of superoxide, peroxynitrite, and carbon dioxide, Free Radic. Biol. Med. 25 (4–5) (1998) 392–403.
[54] S.V. Lymar, J.K. Hurst, Rapid reaction between peroxonitrite ion and carbon dioxide: implications for biological activity, J. Am. Chem. Soc. 117 (34) (1995) 8867–8868.
[55] S.V. Lymar, J.K. Hurst, Carbon dioxide: physiological catalyst for peroxynitrite-mediated cellular damage or cellular protectant? Chem. Res. Toxicol. 9 (5) (1996) 845–850.
[56] G.V. Buxton, C.L. Greenstock, W.P. Helman, A.B. Ross, Critical review of rate constants for reactions of hydrated electrons, hydrogen atoms and hydroxyl radicals (· OH/· O− in aqueous solution, J. Phys. Chem. Ref. Data 17 (2) (1988) 513–886.
[57] P. Neta, R.E. Huie, A.B. Ross, Rate constants for reactions of inorganic radicals in aqueous solution, J. Phys. Chem. Ref. Data 17 (3) (1988) 1027–1284.
[58] N. Hogg, V.M. Darley-Usmar, M.T. Wilson, S. Moncada, Production of hydroxyl radicals from the simultaneous generation of superoxide and nitric oxide, Biochem. J. 281 (2) (1992) 419–424.
[59] L.A. Abriata, A. Cassina, V. Tortora, M. Marin, J.M. Souza, L. Castro, A.J. Vila, R. Radi, Nitration of solvent-exposed tyrosine 74 on cytochrome c triggers heme iron-methionine 80 bond disruption. Nuclear magnetic resonance and optical spectroscopy studies, J. Biol. Chem. 284 (1) (2009) 17–26.
[60] R.T. Hamilton, L. Asatryan, J.T. Nilsen, J.M. Isas, T.K. Gallaher, T. Sawamura, T. K. Hsiai, LDL protein nitration: implication for LDL protein unfolding, Arch. Biochem. Biophys. 479 (1) (2008) 1–14.
[61] V.N. Uversky, G. Yamin, L.A. Munishkina, M.A. Karymov, I.S. Millett, S. Doniach, Y.L. Lyubchenko, A.L. Fink, Effects of nitration on the structure and aggregation of alpha-synuclein, Brain Res, Mol. Brain Res. 134 (1) (2005) 84–102.
[62] M. Gao, D. Craig, O. Lequin, I.D. Campbell, V. Vogel, K. Schulten, Structure and functional significance of mechanically unfolded fibronectin type III1 intermediates, in: Proc. Natl. Acad. Sci. U. S. A, vol. 100, 2003, pp. 14784–14789, 25.
[63] R. Bascetin, K. Admane, R. Agniel, T. Boudou, T. Doussineau, R. Antoine, O. Gallet, J. Leroy-Dudal, C. Vendrely, Amyloid-like aggregates formation by blood plasma fibronectin, Int. J. Biol. Macromol. 97 (2017) 733–743.
[64] S.V. Litvinovich, S.A. Brew, S. Aota, S.K. Akiyama, C. Haudenschild, K.C. Ingham, Formation of amyloid-like fibrils by self-association of a partially unfolded fibronectin type III module, J. Mol. Biol. 280 (2) (1998) 245–258.
[65] X. Zhan, X. Wang, D.M. Desiderio, Mass spectrometry analysis of nitrotyrosine-containing proteins, Mass Spectrom. Rev. 34 (4) (2015) 423–448.
[66] K.S. Midwood, L.V. Williams, J.E. Schwarzbauer, Tissue repair and the dynamics of the extracellular matrix, Int. J. Biochem. Cell Biol. 36 (6) (2004) 1031–1037.